Eur. Phys. J. E **25**, 163–173 (2008)
DOI 10.1140/epje/i2007-10277-1

THE EUROPEAN PHYSICAL JOURNAL E

Phase behavior of flowerlike micelles in a SCF cell model

J. Sprakel[1,2,a], N.A.M. Besseling[3], M.A. Cohen Stuart[1], and F.A.M. Leermakers[1]

[1] Laboratory of Physical Chemistry and Colloid Science, Wageningen University, Dreijenplein 6, 6703 HB, Wageningen, the Netherlands
[2] Dutch Polymer Institute (DPI), P.O. Box 902, 5600 AX Eindhoven, the Netherlands
[3] Delft University of Technology, Department of Chemical Engineering, Section NanoStructured Materials, Julianalaan 136, 2628 BL Delft, The Netherlands

Received 3 October 2007 and Received in final form 16 January 2008
Published online: 10 March 2008 –

Abstract. We study the interactions between flowerlike micelles, self-assembled from telechelic associative polymers, using a molecular self-consistent field (SCF) theory and discuss the corresponding phase behavior. In these calculations we do not impose properties such as aggregation number, micellar structure and number of bridging chains. Adopting a SCF cell model, we calculate the free energy of interaction between a central micelle surrounded by others. Based on these results, we predict the binodal for coexistence of dilute and dense liquid phases, as a function of the length of the hydrophobic and hydrophilic blocks. In the same cell model we compute the number of bridges between micelles, allowing us to predict the network transition. Several quantitative trends obtained from the numerical results can be rationalized in terms of transparent scaling arguments.

PACS. 64.75.Yz Self-assembly – 64.75.Xc Phase separation and segregation in colloidal systems – 31.15.xr Self-consistent-field methods

1 Introduction

Telechelic associative polymers are solvophilic linear polymers modified with a solvophobic group or block at both ends of the chain. The central block can, *e.g.*, be a neutral polymer such as poly(ethylene oxide) [1] and poly(acryl amide) [2] or a polyelectrolyte [3]. Also for the end groups a wide variety of choices exist, such as alkyl tails [1,2], perfluoro-alkyl tails [4], pyrene groups [5], hydrophobic polymer blocks such as poly(propylene oxide)s [6] and even buckminsterfullerenes [7].

When two layers of end-adsorbed telechelic polymers (also known as telechelic brushes), are brought close to each other, bridges between the two surfaces will form. As chains gain conformational freedom when they can form bridges in addition to forming loops, an entropic attraction between the brushes results. Early numerical investigations by Milner and Witten [8] revealed that the overall interaction potential between these types of brushes is a balance between steric repulsion and a weak bridging attraction, both appearing at distances of the order of twice the brush thickness. A recently published study, using density functional theory, substantiates these conclusions [9]. There is also experimental evidence of bridge formation between end-adsorbed layers of telechelic polymers [10,11].

Bridging also occurs between micelles of telechelic associative polymers and leads to the formation of transient networks, but can also cause a demixing into a dilute and a more concentrated liquid phase [12]. The depth of the attractive well in the pair potential between these flowerlike micelles is reported to depend primarily on the aggregation number and on the degree of stretching of the coronal chains [13]. For ideal chains, the possibility to form bridges increases the conformational possibilities with a factor of 2 per chain. This leads to an increase in the entropy per chain of $k_B \ln 2 = 0.69 k_B$, hence a change in free energy of $-0.69 k_B T$ per chain. For chains with excluded volume, steric effects also come into effect, and as a result the effective contribution, per chain, to the attraction is reduced [14].

Based on theoretical predictions for the pair potential, several descriptions are available that link the compositions in the dilute and the dense coexisting phases to the molecular architecture [15,16]. For associative polymers bearing many associating groups per chain it is predicted that, in the absence of excluded-volume interactions, all solutions are unstable above the network threshold and therefore must phase separate [17]. For telechelic associative polymers, with only 2 associating groups per chain, we will show that formation of a transient network is not

[a] e-mail: joris.sprakel@wur.nl

necessarily accompanied by phase separation. This is also suggested by experiments on alkyl end-capped poly(ethylene oxide)s [16].

In a previous study we have used the self-consistent field theory of Scheutjens and Fleer in combination with scaling arguments to investigate some important aspects of the self-assembly of telechelic associative polymers into spherical flowerlike micelles [18], such as the entropic penalty associated with the formation of loops in the corona. In this paper we extend this work in studying the interactions between flowerlike micelles, and two of the macroscopic consequences of these interactions; phase separation and network formation. Our method differs from previous efforts to model the interactions between these micelles. We choose a more "*ab initio*" approach; we do not make *a priori* assumptions on the micellar structure and aggregation number, instead these follow from our analysis.

We will start from the free energy of interaction between a central micelle surrounded by others, calculated in a so-called cell model. Subsequently, we use these results to predict the coexistence curves for dilute and dense micellar phases. Finally, we briefly discuss the threshold where intermicellar bridging leads to the formation of a transient network, which can also be predicted from the self-consistent field calculations. Several trends from the numerical results will be explained using scaling arguments based on the molecular architecture of the telechelic polymers.

2 Self-consistent field cell model for micelles

Our calculations are based on the discrete self-consistent field theory developed by Scheutjens and Fleer (SF-SCF) [19,20]. In SF-SCF theory the same length a is used to divide chains into segments and space into lattice sites. We consider telechelic chains, with segments $s = 1, 2, \ldots, N$, and a spherical lattice consisting of h concentric layers with reflecting boundary conditions. The spherical lattice will be referred to as the "cell" in the remainder of this paper. The mean-field approximation is applied to each layer z with $z = 1, 2, \ldots, h$, hence the micelles are spherical. The key lattice parameters are the number of sites $L(z)$ in each layer, for our spherical geometry $L(z) = \frac{4}{3}\pi(z^3 - (z-1)^3)$, and the *a priori* step probabilities $\lambda_{\Delta z}(z)$. These step probabilities are given by the fraction of all neighboring sites of a site in layer z that are located at $z + \Delta z$ ($\Delta z = -1, 0, +1$) and reflect the probability that a segment $s-1$, linked to a segment s located at z, is in layer $z + \Delta z$. In a curved geometry, the step probabilities are a function of z and obey the internal balance: $\lambda_{-1}(z)L(z+1) = \lambda_1(z)L(z)$ [21]. Nearest-neighbor interactions are taken into account in terms of the Flory-Huggins interaction energy that is parameterized by the interaction parameters χ_{xy}, where x and y represent any two different segment species [22].

In the context of this model we can define a molecular state c of a species i, by the subsequent z-positions of all chain segments z_{is}^c. The number of possible conformations ω_i^c of a chain i in state c is, within a Markov approximation, given by

$$\omega_i^c = L(z_{i1}^c) \prod_{s=2}^{N_i} \lambda_{\Delta z}(z_{is}^c) Z, \tag{1}$$

where z_{is}^c is the layer in which segment s of molecule i in state c is found, $L(z_{i1}^c)$ is the number of sites in layer z, where the first segment of species i in conformation c is located, and Z is the number of neighbors of each site. $\prod_{s=2}^{N} \lambda_{\Delta z}(z_{is}^c)$ is the multiple product of the step probabilities of the subsequent steps, going from the layer where segment 1 is located to the layer where segment 2 is located, etc. up to the last segment N_i, all according to the conformation c.

The Helmholtz energy of the inhomogeneous system can be written as a functional of the distribution of molecular states;

$$\frac{F(\{n_i^c\}, T)}{k_B T} = \sum_{i,c} n_i^c \ln\left(\frac{n_i^c}{\omega_i^c}\right) + \frac{F^{int}}{k_B T}. \tag{2}$$

The first term accounts for the configurational entropy. The Flory-Huggins interaction energy is given by the second term, and can be written as

$$\frac{F^{int}}{k_B T} = \frac{1}{2} \sum_{z,x,y} n_x(z) \langle \phi_y(z) \rangle \chi_{xy} + u'(z) \left[\sum_x n_x(z) - L(z) \right], \tag{3}$$

in which $n_x(z)$ is the number of segments of segment species x in layer z. The factor $\langle \phi_y(z) \rangle$ is the average fraction of y-segments among the nearest neighbors of a segment in layer z and is found with $\langle \phi_y(z) \rangle = \sum_{\Delta z} \lambda_{\Delta z}(z) \phi_y(z)$ where $\varphi_y(z) = n_y(z)/L(z)$. The second term in equation (3) is coupled to the incompressibility of the system, in which $u'(z)$ is the Lagrange parameter.

The abundance of each molecular state in terms of a molecular field is obtained by evaluating $\partial \Omega / \partial n_i^c = 0$ ($\forall i, c$), with the grand potential

$$\Omega = F - \sum_i \mu_i n_i, \tag{4}$$

where $\mu_i = (\partial F / \partial n_i)_{T, n_{j \neq i}}$. The number of molecules of species i in state c, n_i^c, is found from a Boltzmann weight of the potential fields for that species u_i^c, and follows

$$n_i^c \propto \omega_i^c \exp\left[\frac{-u_i^c}{k_B T}\right]. \tag{5}$$

The potential field for a species i in conformation c, follows from summation over the segment potentials $u(z_{is}^c)$ for all segments in the chain:

$$u_i^c = \sum_{s=1}^{N_i} u(z_{is}^c). \tag{6}$$

The segment potential for a segment s of type x in layer z is obtained by differentiating the interaction term in the

free energy (Eq. (3)) to the number of segments of type x in that layer: $u_x(z) = \partial F^{int}/\partial n_x(z)$.

A solution for the complete distribution of molecular states $\{n_i^c\}$ should satisfy the following incompressibility constraints: $\sum_x n_x(z) = L(z)$ for all z's, which fixes $u'(z)$, and $\sum_c n_i^c = n_i$ for all i's, which gives the normalization constant for equation (5).

It turns out that the segment density distributions, that determine the molecular field, can be found using the propagator scheme developed by Scheutjens and Fleer [19] without explicitly evaluating all n_i^c's. In this way both the molecular fields and the segment density distributions can be efficiently calculated in a numerical iteration procedure, until self-consistency is reached [23]. A more detailed description of SF-SCF theory and its applications to self-assembly can be found elsewhere [24]

In a previous study on the micellization of telechelic polymers we have used a molecularly realistic model to predict the self-assembly of a specific class of telechelic associative polymers, *i.e.* alkyl end-capped poly(ethylene oxide)s, in which hydrogenated carbon atoms and ether oxygens of poly(ethylene oxide) were treated as different segment types [18]. Here we choose a coarse-grained version of that model, in which the solvophilic, middle-block segments are represented by one "average" segment type B, and the solvophobic, end-block segments are represented by segment type A, such that the present study is applicable to a wide variety of telechelic associative polymers. Freely jointed A-B-A chains are placed on the spherical lattice together with a monomeric solvent S. The A-blocks are oligomeric (N_A between 10 and 35) and strongly segregate with the monomeric solvent. The central B-blocks are polymeric (N_B between 100 and 10000). The interactions between the three segment species are quantified by the corresponding χ parameters. All calculations are carried out under θ-conditions for the polymer backbone, *i.e.* $\chi_{BS} = 0.5$. For example for poly(ethylene oxide), one of the most used neutral backbones in associative polymers, it is known that the Flory interaction parameter between the polymer and water at room temperature is very close to 0.5 [25]. The other two parameters were chosen such that the results for the critical micelle concentrations (CMC) of the molecularly realistic model in [18] are reproduced. The results from the earlier model could be reproduced, with an error of less than 10% for the investigated range of block lengths, with $\chi_{AS} = 1.9$ and $\chi_{AB} = 1$ in the present coarse-grained model. The correspondence between the results for the CMC from the molecularly realistic model [18] and the current model is illustrated in Figure 1.

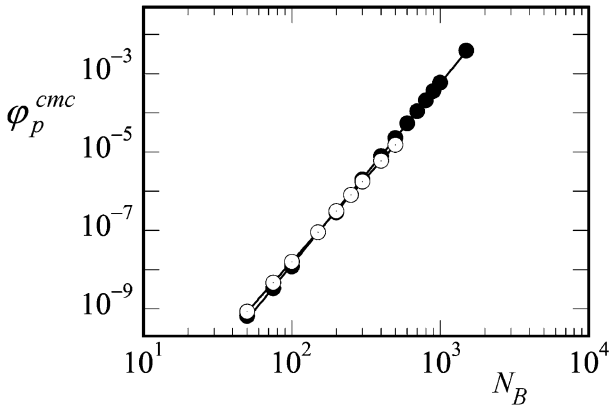

Fig. 1. Comparison between the numerical results for the critical micelle concentration for A_{20}-B_N-A_{20} chains using the present coarse-grained model for telechelic polymers (filled symbols) and the molecularly realistic model used in [18] (open symbols).

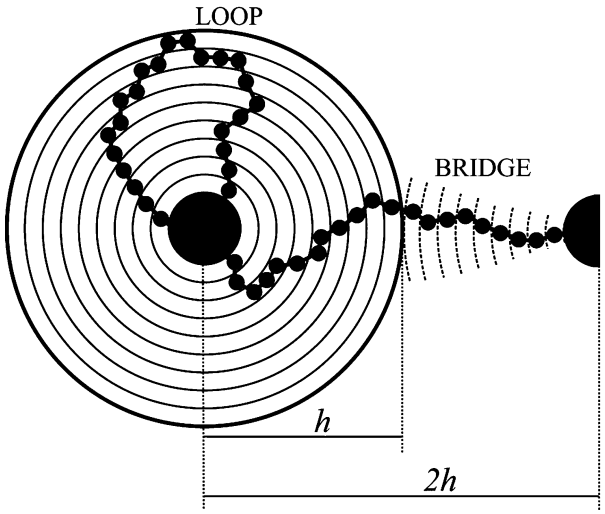

Fig. 2. Schematic representation of the self-consistent field cell model, at a cell size h, with reflecting boundary conditions. Coronal chains, departing from the micellar core, have two "dominant" configurations: i) loops, for all values of h, the one shown here just reaches the outer layer and ii) bridges, that cross the cell boundary, for not too large values of h.

2.1 Isolated, non-interacting micelles

Isolated micelles are studied in the self-consistent field cell model for large values of h, such that the central object cannot interact with any neighbors. For large h, no bridges can form, and all chains form loops (see Fig. 2).

According to the thermodynamics of small systems [26, 27], the work associated with the formation of micelles $\mathcal{E}$ must vanish, *i.e.* $\mathcal{E} = 0$. In a real system, the number of micelles $\mathcal{N}$ is adjusted by the system until this condition is met, *i.e.* $\partial F/\partial \mathcal{N} = \mathcal{E} = 0$. In this sense, the number of micelles is not a controlled variable (*i.e.* it is not an external variable). In the self-consistent field modeling of flowerlike micelles, however, one studies a small system that contains a single micelle. Indeed, for such an analysis the number of micelles is exactly controlled. This implies that the thermodynamic analysis of micellization in a SCF model requires special attention.

The micellar object in the SCF model is translationally restricted to the center of the coordinate system. The grand potential Ω of such a micelle is readily available from the SCF calculations (see Eq. (4)). For dilute solutions one can estimate the translational entropy per

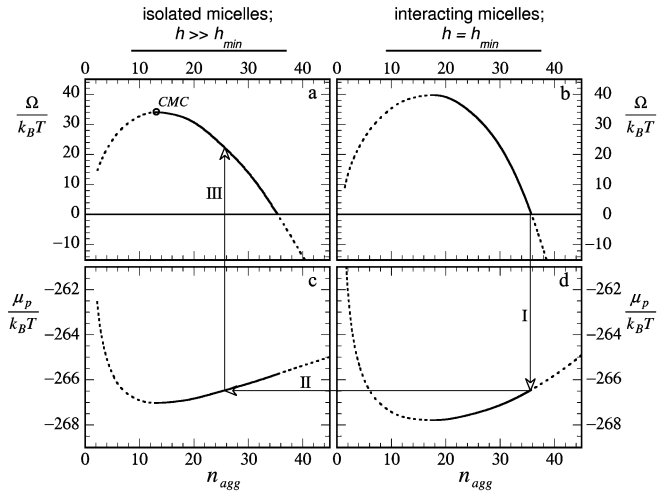

Fig. 3. Typical results from the SF-SCF calculations for isolated and non-interacting micelles ($h \gg h_{min}$, a and c) and for interacting micelles at the minimum of the interaction energy between the micelles with respect to h ($h = h_{min}$, b and d). Results shown are for systems of A_{20}-B_{500}-A_{20} polymers, dotted lines represent solutions that are not macroscopically stable.

micelle as $S_{trans} = -k_B \ln \varphi_p^m$, where φ_p^m is the volume fraction of micelles in the system. The overall work of formation of a micelle in the SCF model is therefore

$$\mathcal{E} = k_B T \ln \varphi_p^m + \Omega = 0, \tag{7}$$

which gives the connection between the microscopic model to the macroscopic thermodynamics [26,27]. In the SCF model, equation (7) is used as follows. Typically from the calculations the relation $\Omega(n_{agg})$ is known, where n_{agg} is the excess number of amphiphiles per micelle. From equation (7) we then find $\varphi_p^m(n_{agg})$. As $0 < \varphi_p^m < 1$, it is clear that relevant micelles have $\Omega > 0$.

It can be shown that the Gibbs-Duhem equation for micellization in the small system reads

$$\partial\Omega/\partial\mu_p = -n_{agg}. \tag{8}$$

As the fluctuations in (micellar) aggregation numbers are related to $\partial n_{agg}/\partial\mu_p$, and because this is necessarily a positive number, we find from equation (8) that relevant micellar systems obey to $\partial\Omega/\partial n_{agg} < 0$ (stability constraint). In the context of this SCF model, the critical micelle concentration is defined as the concentration where $\partial\Omega/\partial n_{agg} = 0$. From equation (7) and Figure 3, it follows that the concentration of micelles at the critical micelle concentration is very small. This is consistent with the classical view of micellization, as, *e.g.*, explained in [28].

The aggregation number n_{agg} is defined as the number of polymer chains in the micelle, and is related to the total number of polymer chains n_p in the system and the number of micelles $\mathcal{N}$ with $n_p = \mathcal{N} n_{agg} + V\varphi_p^b/N$, where V is the volume of the system, φ_p^b is the bulk unimer concentration and N is the total chain length of the polymer. For the calculations, where $\mathcal{N} = 1$, the appropriate volume is the cell volume $V^{cell} = \frac{4}{3}\pi h^3$.

In Figure 3a we see the grand potential as a function of aggregation number, due to the stability constraint we only consider the solutions for which $\partial\Omega/\partial n_{agg} < 0$. In Figure 3 all solutions from the self-consistent field calculations, which correspond to situations that are not macroscopically stable, *i.e.* when $\partial\Omega/\partial n_{agg} > 0$, or which are physically not meaningful, *i.e.* when $\Omega < 0$, are indicated with dotted lines.

2.2 Interacting micelles in concentrated systems

The interactions between micelles are studied in the cell model by decreasing the cell size h to the same order of magnitude as the size of the micelle. Typical results for this situation are shown in Figures 3b and 3d. Here again we only consider those solutions for which $\partial\Omega/\partial n_{agg} < 0$. By decreasing the cell size, which is equivalent to increasing the concentration of micelles, the central object can interact with its neighbors by way of the reflecting boundary conditions. In essence the idea of a reflecting, *i.e.* mirroring, boundary, is straightforward. In a flat geometry, the reflecting boundary is a plane of symmetry; for each chain configuration that leaves the system volume through the boundary, a complementary chain enters the volume through the same boundary. Mathematically this is implemented by forcing the segment densities, as well as the segment potentials, in a given layer outside the boundary to assume the same (known) value as its mirror-image inside the volume. The mathematical implementation of the boundary condition in the current spherical geometry is the same. An intuitive understanding of the resulting situation is, however, somewhat troublesome. Again, for each chains that leaves the cell through the outer boundary a complementary chain enters the volume as if it comes from a neighboring micelle. The exact position of all neighbors is however not realistically accounted for. The distance between the center of the central micelle and its mirror images is $2h$. For small enough values of h we distinguish two dominant types of conformations of the coronal parts of the polymers upon interaction; bridges and loops. This is illustrated schematically in Figure 2.

We compute the thermodynamic quantities for these interacting micelles at $\Omega = 0$ as a function of h. As discussed in the previous section the grand potential is directly coupled to the translational entropy of the micelles (Eq. (7)). Setting the condition $\Omega = 0$ implies that we consider the translational entropy to be negligible. At high concentrations, where the micelle interacts with many neighbors, this assumption is reasonable. It is known that under experimental conditions a structured and highly interconnected micellar network is formed, in which the translational freedom of the micelles is obviously suppressed [29]. One of the consequences of the cell model,is that the distances between all micelles in the system are approximated to be equal. We can argue that this approximation should be reasonable for concentrated systems where the micelles are closely packed, and for systems where the micelles are trapped in an attractive well that is many times larger than the thermal energy $k_B T$,

such that fluctuations around the equilibrium position are small. This issue is evaluated in somewhat more detail in the Discussion at the end of this paper.

The free energy difference of a micelle surrounded by neighbors with respect to an isolated micelle (for which $\Omega = 0$), is defined as $\Delta F^m(h) = F^m(h) - F^m(\infty)$. Note that this free energy difference is not a pair potential, rather the interaction free energy between a central micelle and all its neighbors. The cell size value where ΔF_m is minimal is denoted h_{min}.

2.3 Computing biphase coexistence

The attractive interactions between flowerlike micelles can cause macroscopic demixing [12]. To determine the coexistence in the context of this SCF model we make two approximations. The first is that in the dilute phase the micelles have no intermicellar interactions, such that we can use the results for isolated micelles to predict the properties of this phase. The second approximation is that in the dense phase the micelles have no translational entropy, such that we can use the results from the cell model for intermicellar interactions for this phase. These approximations are likely to be valid away from the critical point. Close to the critical point however, the micelles will interact with each other in both phases as well as have significant translational entropy in both the dense and the dilute phase. The true position of the critical point is therefore not obtained in this approach.

In the coexisting liquid phases (denoted *dense* and *dilute*) both the osmotic pressures ($\Pi^{dense} = \Pi^{dilute}$) and the chemical potential of the polymer ($\mu_p^{dense} = \mu_p^{dilute}$) should be equal. For the dilute phase we can argue that, as the concentration of micelles is very low, the osmotic pressure will be negligible. Here we approximate the osmotic pressure to be zero. Consequently, the osmotic pressure in the dense phase will also be zero. Although the concentration of micelles is significant in the dense phase, we can argue that the attraction between the micelles, resulting in a negative second virial coefficient, can strongly reduce the osmotic pressure to negligible values. To predict coexistence we need to find solutions to the self-consistent field model for both isolated and interacting micelles, that have the same chemical potential of the polymer μ_p.

Our approach is schematically illustrated in Figure 3. We start with the typical result of the grand potential *versus* aggregation number for interacting micelles (dense phase). Above we discussed the choice for approximating the osmotic pressure to be zero in both phases. For an incompressible system, as is the case in these SCF calculation, we can find the osmotic pressure by differentiating the free energy to the cell volume, that is given by $\frac{4}{3}\pi h^3$, hence

$$\Pi = \frac{-\partial F^m(h)}{\partial V} = \frac{-\partial F^m(h)}{4\pi h^2 \partial h} = 0. \tag{9}$$

Since $4\pi h^2$ is always finite positive, $\partial F^m/\partial h$ must be zero. As a consequence, we will regard the minimum of the free energy of interaction with respect to h to be the equilibrium situation. In other words, we find the solutions to the self-consistent field model for $h = h_{min}$ and for which $\Omega = 0$. These requirements are met, as indicated in Figure 3b, for a given aggregation number (here $n_{agg} = 34$). In the plot of the chemical potential of unimers μ_p *versus* aggregation number (Fig. 3d) we can now find the corresponding chemical potential of the polymer chains in the bulk phase (here $-266.5 k_B T$, arrow I).

The volume fraction in the dense phase (φ_p^{dense}), given by the composition in the cell, can be split up into two contributions: that of polymer chains that are associated in the central micelle (φ_p^m) and that of free unimers (φ_p^b). The contribution of chains in the micelle, φ_p^m, is obtained by dividing the total number of polymer segments (each occupying 1 lattice site) in the micelle by the cell volume $V^{cell} = \frac{4}{3}\pi h_{min}^3$;

$$\varphi_p^m = \frac{N_p n_{agg}}{\frac{4}{3}\pi h_{min}^3}, \tag{10}$$

where $N_p = 2N_A + N_B$ is the total chain length of the ABA polymer. The bulk volume fraction of free unimers follows from μ_p, using the Flory-Huggins expression for the chemical potential for a system composed of species S (solvent) and ABA (polymer) and segments S, A and B;

$$\frac{\mu_p - \mu_p^*}{k_B T} = -\ln \varphi_p^b + (1 - \varphi_p^b)(1 - N_p) + \\ + \frac{1}{2} N_p \sum_i \sum_j (\varphi_i^b - \Phi_i)\chi_{ij}(\varphi_j^b - \Phi_j), \tag{11}$$

in which μ_p^* is the reference state of the chemical potential of the polymer, defined such that equation (11) returns zero for $\varphi_p^b = 1$. φ_i^b and φ_j^b are the bulk volume fractions of segment types i and j, with i or $j = A, B, S$. Φ_i and Φ_j are the fractions of segments in ABA the polymer that are of type i and j respectively. Hence, Φ_S is zero, $\Phi_A = 2N_A/N_p$ and $\Phi_B = N_B/N_p$.

Now that we have all ingredients to compute the composition of the dense phase, we proceed to calculate the composition of the dilute phase. We now start from the chemical potential of the unimers found in Figure 3d (arrow I). As the chemical potential of the unimers must be equal in both phases, we can find the coexisting configuration of a system of isolated non-interacting micelles. In Figure 3c we see that at the given chemical potential, the isolated micelles have an average aggregation number of 25 (arrow II). For the dilute system we can now also see, in Figure 3a, that at this chemical potential and corresponding configuration, the micelles have a finite, non-zero grand potential (arrow III), in this case $\Omega \approx 20\ k_B T$. This indicates that in the dilute phase the micelles do have significant translational entropy, since $\Omega = -S_{trans} T$.

With the chemical potential and the grand potential known for the dilute phase, we can also calculate its overall composition. Again, the overall polymer volume fraction is given by $\varphi_p^{dilute} = \varphi_p^b + \varphi_p^m$. The bulk volume fraction φ_b^b again follows from equation (11), and must be the same as in the dense phase since the chemical potentials are also equal. The volume fraction of polymer in micelles in the dilute phase can be obtained from Ω (Eq. (7)).

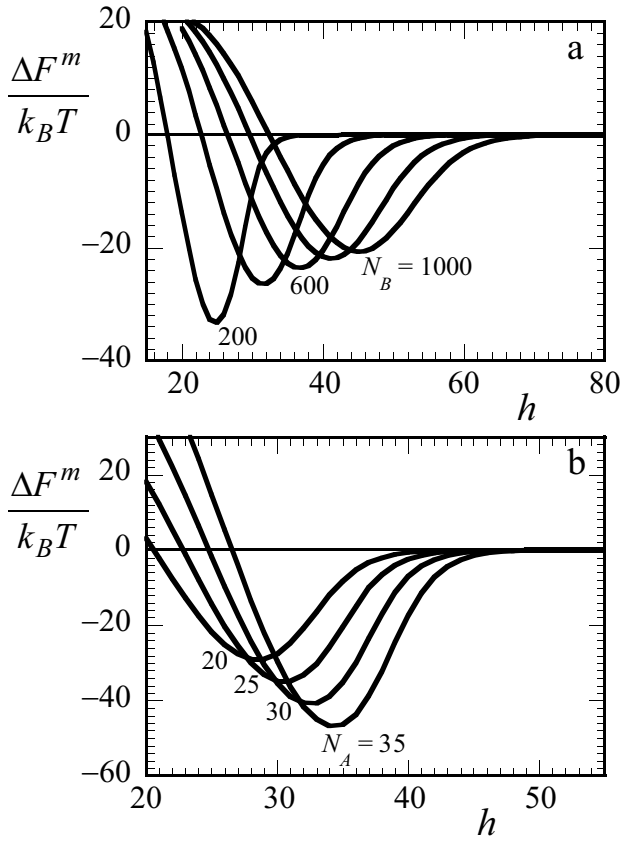

Fig. 4. Free energy of interaction $\Delta F^m(h)$ between a central flowerlike micelle and all its neighbors, calculated in the self-consistent field cell model; a) for A_{20}-B_N-A_{20} polymers with N_B = 200, 400, 600, 800 and 1000 and b) for A_N-B_{500}-A_N with N_A = 20, 25, 30 and 35.

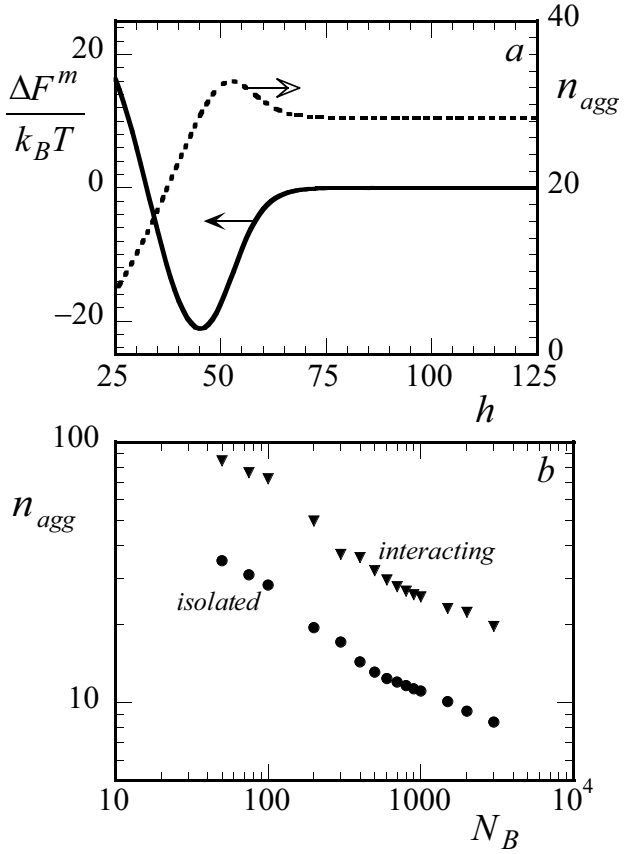

Fig. 5. a) Effect of interactions in the cell model on the aggregation number (n_{agg}), in comparison to the interaction free energy ΔF^m for A_{20}-B_{800}-A_{20} polymers and b) dependence of the aggregation number on the backbone length for isolated micelles ($h \gg h_{min}$, circles) and micelles at the minimum of the interaction potential ($h = h_{min}$, triangles).

2.4 Computing the number of bridging chains

In this SCF cell model it is also possible to obtain the number of bridges n_b that are formed by a micelle. To find n_b we start by defining the lattice parameters for the central object and its mirror image. The system now contains twice as many layers; $z = 1, 2 \ldots h, h+1 \ldots 2h$. The number of sites per layers $L(z)$ is given by $L(z) = \frac{4}{3}\pi(z^3 - (z-1)^3)\ \forall\ z < h+1$ and $L(z) = L(2h-z+1)\ \forall\ z > h$. Consequently, we need to mirror the step probabilities, such that for $z > h$: $\lambda_{\Delta z}(z) = \lambda_{-\Delta z}(2h-z+1)$ ($\Delta z = -1, 0, 1$), and the segment potentials, with $u_x(z) = u_x(2h-z+1)$ for all $z > h$ and x. By defining a bridge as a chain that has its first segment in a layer with $z < h+1$ and its last segment in $z > h$, we can calculate n_b using the propagator scheme of Scheutjens and Fleer.

3 Intermicellar interactions

Several results for the interactions between flowerlike micelles, calculated in the SCF cell model, are shown in Figure 4, as a function of backbone length (Fig. 4a) and end-block length (Fig. 4b). We can recognize some clear trends: the interactions decrease in strength and increase in range with increasing backbone length and with decreasing length of the associating end blocks.

For end-adsorbed layers of telechelic polymers it has been predicted that the *range* of both steric and bridging interactions is proportional to the brush thickness [8]. For micelles this suggests that the interaction range is characterized by the radius of the micelle (R) [13]. We have previously shown [18] that

$$R \propto \left(N_B + {n_{agg}}^{\frac{1}{6}} N_A^{\frac{2}{3}}\right)^{\frac{1}{2}} {n_{agg}}^{\frac{1}{4}}. \qquad (12)$$

This follows from the Daoud-Cotton model [30], adjusted for the non-zero size of the micellar core. When the concentration of micelles is increased, or, in other words, when the typical distance between the micelles is decreased, the chemical potential changes. This also leads to a change in aggregation number. In Figure 5a the change in aggregation number with h is shown (dotted curve). We see a significant change of the number of chains per micelle with decreasing h that is equivalent to increasing the concentration of micelles. This implies that, to properly apply equation (12) we must use $n_{agg}(h)$ rather than a fixed n_{agg}. In

Figure 5b it is shown that although the absolute value of n_{agg} depends on the concentration, the same dependence between aggregation number and backbone length is found for isolated micelles and micelles that interact with multiple neighbors. The change in aggregation number with a variation in the molecular architecture has been discussed previously [18].

Adopting a Derjaguin approximation, Meng and Russel calculate the interactions between flowerlike micelles starting from the results for flat telechelic brushes. Within this approximation, the *strength* of the interaction is governed by two parameters only; the aggregation number n_{agg} and the degree of stretching of the coronal chains $RN_B^{-1/2}$. They derive that $\Delta F^m \propto n_{agg} N_B R^{-2}$. For R we can use equation (12). Here we can approximate R by $N_B^{1/2} {n_{agg}}^{1/4}$, since N_B is generally much larger than ${n_{agg}}^{1/6} N_A^{2/3}$. Rewriting gives

$$\Delta F^m(h) \propto n_{agg}(h) \frac{N_B}{R^2} \approx n_{agg}(h)^{\frac{1}{2}}. \qquad (13)$$

With equations (12) and (13) as predictions for the range and strength of the interactions respectively, we can plot the curves in Figure 4 on rescaled coordinates. We plot the normalized interaction energy $\Delta F^m/\sqrt{n_{agg}}$ *versus* the normalized distance between the centers of the micellar objects h/R, where R is found from equation (12). The result is shown in Figure 6.

We see that the curves, with the exception of the curves for $N_B = 200$ in Figure 6a, now almost collapse onto a master curve. This confirms that the range of the interactions is determined by the size of the micelles and that the strength of the interactions is a function of the aggregation number and chain stretching only. The curve for the smallest middle block length ($N_B = 200$) in Figure 6a does not coincide with the other curves because the assumption that ${n_{agg}}^{1/6} N_A^{2/3}$ is negligible compared to N_B (see derivation of Eq. (13)) is not valid for this short-chain length.

If we take the value of the interaction energy at h_{min} and divide this by the aggregation number, we find the contribution per chain to the depth of the attractive well. In the range of molecular parameters investigated here, we find an average contribution per chain to the attraction of 0.6–0.7 k_BT. This is of the same order of magnitude as the predicted value of $k_BT \ln 2 = 0.69\ k_BT$ for ideal chains [13]. We must note that, although we are at θ-conditions for the polymer backbone ($\chi_{BS} = 0.5$), the chains do show stretching in the micellar corona. This is also reflected in the fact that for micelles of ideal chains the depth of the minimum would depend solely on the aggregation number, whereas here we need to account for chain stretching as well in order to collapse the curves in Figure 6. We can attribute this apparent importance of excluded-volume effects for chains in a θ-solvent, to crowding in the corona of the micelle.

The interactions start when h/R is approximately unity, which corresponds to a separation between the centers of the interacting objects of roughly twice the micellar radii. This has also been predicted previously [8].

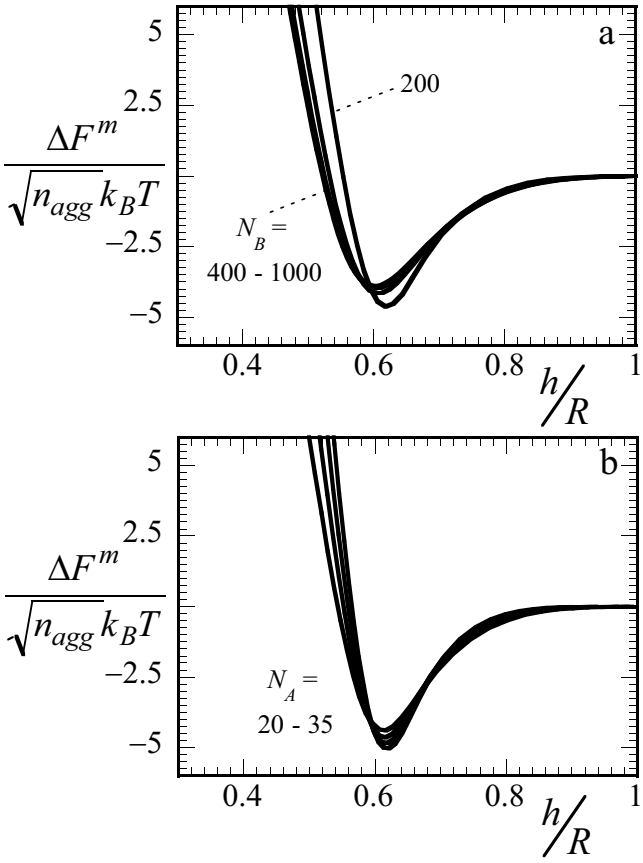

Fig. 6. Rescaled free energy of interaction between a central flowerlike micelle and all its neighbors, calculated in the self-consistent field cell model, plotted *versus* the rescaled cell size h/R; a) for A_{20}-B_N-A_{20} polymers with N_B ranging from 200 to 1000 and b) for A_N-B_{300}-A_N with N_A ranging from 30 to 35.

4 Biphase coexistence

In Figure 7 we show the numerically calculated coexisting compositions (Eqs. (7), (10) and (11)) in systems of flowerlike micelles, both as a function of the length of the middle B-block and as a function of the length of the A-end-blocks. We can immediately see that the phase diagrams are strongly asymmetric with respect to the volume fraction of polymer at the extrapolated critical point.

In the concentrated phase the amount of unimers is negligible compared to the chains assembled in the micelle, hence $\varphi_p^{dense} \approx \varphi_p^m$. Also $N_p \approx N_B$ as the end-block length is small compared to the middle block in the molecular architectures investigated here. We already argued that $h_{min} \propto R$. Using equation (10) we can derive

$$\varphi_p^{dense} \propto \frac{n_{agg} N_B}{R^3}. \qquad (14)$$

The proportionality $\varphi_p^{dense} \propto R^{-3}$ was already predicted by Francois *et al.* [16]. The radius of the micelle R can again be approximated by $N_B^{1/2} n_{agg}^{1/4}$. The aggregation number is intricately linked to molecular architecture, as discussed in [18]. As a first-order approximation we can

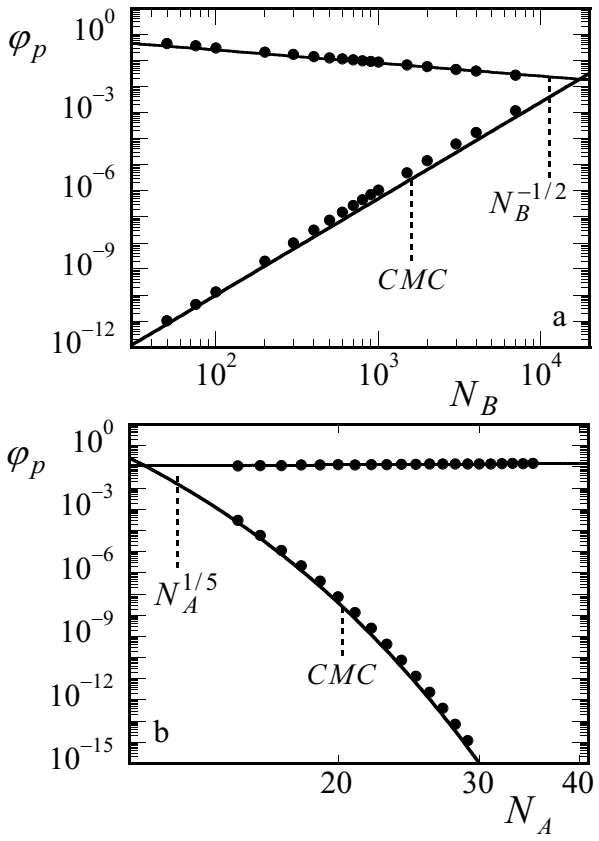

Fig. 7. Numerically obtained binodals (symbols) as a function of a) backbone length (N_B) in a system of A_{20}-B_N-A_{20} polymers and b) end block length (N_A) in a system of A_N-B_{500}-A_N polymers. Solid lines are numerically calculated critical micelle concentrations (CMC) and fits to the scaling relation in equation (15), with $\varphi_p \propto N_B^{-1/2}$ in a) and $\varphi_p \propto N_A^{1/5}$ in b).

use $n_{agg} \propto N_A^{4/5}$, in which the logarithmic dependency of the aggregation number on N_B has been omited as it is much weaker than the power law proportionality between N_A and n_{agg}. We now find

$$\varphi_p^{dense} \propto N_B^{-\frac{1}{2}} N_A^{\frac{1}{5}} . \tag{15}$$

To test this scaling relation, we have fitted the dense branches of the binodals in Figure 7 to $\varphi_{dense} \propto N_B^{-1/2}$ (Fig. 7a) and $\varphi_{dense} \propto N_A^{1/5}$ (Fig. 7b), respectively. An excellent correspondence is found between the scaling argument and the numerical results.

For the dilute branch of the binodal we find that the compositions are close to the critical micelle concentrations (CMC). This can be seen in Figure 7, where the lower solid lines are the critical micelle concentrations. For the parameters chosen here, that imply strong segregation of the end blocks, we have previously [18] discussed the dependency of the CMC on the molecular architecture. Combining $\varphi_{dilute} \approx CMC$ with the result found in [18] gives

$$\varphi_p^{dilute} \propto N_B^{\frac{3}{2}+g} \exp\left(-\frac{3}{2} N_A\right), \tag{16}$$

where the exponential decay of the CMC with the end-block length N_A is similar to that of ordinary surfactants, but twice as strong because there are 2 hydrophobic moieties attached to a single chain. The factor N_B^g is the dependency of the CMC on the length of the hydrophilic block for equivalent diblock copolymers (in these calculations $g \approx 2$), and the factor $N_B^{3/2}$ accounts for the entropy loss due to loop formation of non-interacting telechelic chains in isolated flowerlike micelles [31].

Using the scaling relations for both branches of the binodal in equations (15) and (16) we can also derive expressions for the point where these branches meet. This intersection point can be considered to be an upper limit for the critical value of N_B or a lower limit for the value of N_A at the critical point. For example, to find the upper limit for the critical backbone length (N_B^*), for a given end block length N_A, we start with $\varphi_p^{dense} = \varphi_p^{dilute}$. Rewriting then gives

$$N_B^* \propto N_A^{\frac{1}{10g}} \exp\left(\frac{3}{4g} N_A\right). \tag{17}$$

As the latter, exponential, term grows much faster than the first, power law, term, we can neglect the first term and find; $N_B^* \propto \exp(\frac{3}{4g} N_A)$. Here $g \approx 2$, giving; $N_B^* \propto \exp(\frac{3}{8} N_A)$ This gives a quasi-Traube's rule [32] for the minimal length of a middle block, for a given end block length, that assures that the system is homogeneous at all concentrations, which could be used as a design rule, *e.g.*, for the development of novel associative thickeners, where the occurrence of demixing is undesired.

In the explanation of the approach to compute biphase coexistence, we have mentioned that the model can be expected to be only valid far enough away from the critical point. As explained in more detail in the Discussion-section of this paper, we expect all data points shown in Figure 7 to lie within the validity of our model.

5 Transient network threshold

From the self-consistent field cell model we have also obtained the number of bridges, n_b, formed by the central micelle with its neighbors. As stated in the introduction we expect bridging to be an entropic phenomenon, driven by the gain in conformational freedom when chains have the possibility to form bridges in addition to forming loops. For a chain, of which at least one segment is located at the symmetry plane, the probability to form a loop and the probability to form a bridge are equal. As a result, we expect that at high concentrations exactly half of all chains have formed a bridge, whereas the other half is present in loops. In Figure 8a the fraction of chains that have formed a bridge $\alpha = n_b/n_{agg}$ is plotted *versus* polymer concentration. It shows that in the limit of high concentrations this value indeed levels off at a plateau value of $\frac{1}{2}$. From the same plot we can also conclude that the onset and saturation of bridging occurs at lower volume fractions for chains with larger middle blocks.

Now that we have obtained the number of bridges as a function of polymer concentration we can estimate at what

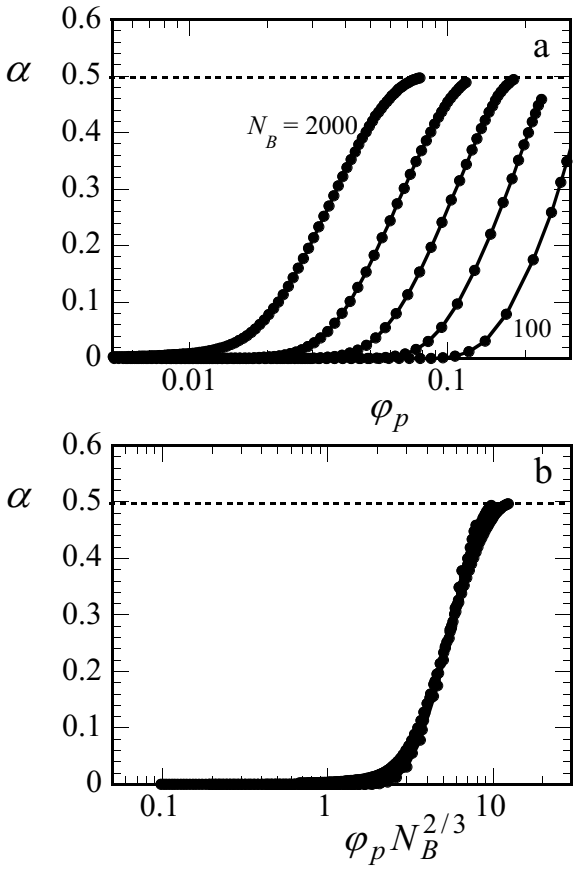

Fig. 8. a) Fraction of the total chains in the micelle that have formed a bridge $\alpha = n_b/n_{agg}$ as a function of polymer volume fraction φ_p for various values of N_B (100, 200, 400, 1000, 2000) in systems of A_{20}-B_N-A_{20} polymers. b) Same results as in a) plotted as α *versus* $\varphi_p N_B^{2/3}$.

concentration a macroscopic association cluster of micelles is formed. Above this concentration, where we have a percolated structure in our system, we can expect the mechanical properties of the system to change from fluid-like to visco-elastic. The concentration φ_p^{net} where this transition occurs is denoted the transient network threshold

To find the network threshold we need to define a criterion for the average number of bridges per micelle that are required for the formation of a macroscopic network (n_b^{net}). Here we will consider two estimates for this transition. The first is the so-called Flory gel point criterion [22], that takes into account the functionality n_{agg} of the nodes;

$$\alpha^{net} = \frac{n_b^{net}}{n_{agg}} = \frac{1}{n_{agg} - 1}\,, \tag{18}$$

where $\alpha^{net} = n_b/n_{agg}$ is the fraction of the total number of possible bridges that must form to obtain a macroscopic network. In these systems $n_{agg} \gg 1$, hence n_b^{net} goes to unity. The Flory criterion does not take into account non-effective bridges, *e.g.* the formation of rings of nodes (micelles) connected by bridges.

The second criterion is derived from classical bond percolation theory. For a 3-dimensional cubic lattice, Monte-

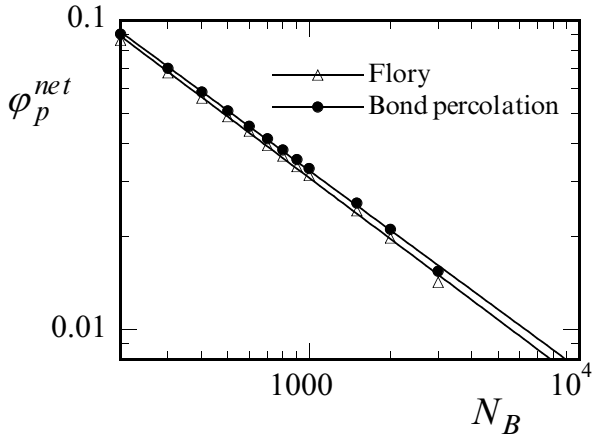

Fig. 9. Comparison between transient network threshold φ_p^{net},as predicted by the Flory-criterion and the bond percolation criterion by Stauffer *et al.* [33] as a function of central block length N_B, for A_{20}-B_N-A_{20} polymers.

Carlo simulations have shown that the fraction of bonds formed should equal 0.25 to reach the bond percolation threshold [33]. As the functionality of the nodes in a 3D cubic lattice is 6 by definition, on average 1.5 bonds/node are required for percolation. In our model we can use this same value for n_b^{net}. This percolation approach does not take into account the functionality of the nodes, rather assumes a fixed value (6 for a 3D cubic lattice), but does account for the formation of non-effective bonds.

The two different criteria are compared in Figure 9. We see, as expected from the definitions of the two criteria, that the predicted transient network thresholds are very close, with the bond percolation criterion giving a slightly higher predicted threshold concentration.

As for the other properties discussed in previous sections, we can investigate how the network threshold changes with variations in the molecular architecture. For the proportionality of φ_p^{net} with the backbone length N_B, we can take a closer look at Figure 9. The solid lines are power law fits to the results from the self-consistent field calculations. We empirically find that $\varphi_p^{net} \propto N_B^{-2/3}$. Using this relation to rescale the volume fraction-axis of Figure 8a, as is done in Figure 8b, we see superposition of all curves of the fraction of bridging chains *versus* concentration. This indicates again that the quantity $N_B^{-2/3}$, for a given N_A, determines the bridge formation throughout the concentration range.

Qualitatively we can understand that the transient network is formed at lower concentrations when the middle block is longer. First of all, the minimal distance required between micelles to allow bridge formation, is larger for larger middle blocks, as the chains can reach over longer distances compared to smaller values of N_B. Secondly, we know from [18] and Figure 5b that the aggregation number is a decreasing function of N_B. If we distribute the same amount of polymer material over many micelles, with a smaller aggregation number, the typical distance between the micelles will be smaller than when we

have few micelles with a large aggregation number. Both effects will contribute to the observed scaling of φ_p^{net} with N_B. At this time however, we do not have a more quantitative explanation for this dependency.

The proportionality of the concentration where a network is formed with the end-block length N_A is more complicated. From our calculations we find that $\varphi_p^{net} \propto N_A^k$, where the scaling exponent k itself is a function of N_B. For the current choice of parameters $k \propto N_B^{0.7}$. The increase in φ_p^{net} with increasing N_A is again attributed to effect that a change in associative block length has on the aggregation number, as we know that $n_{agg} \propto N_A^{4/5}$. How this translates into the intricate relation that is found, is not clear to the authors at present.

In classical transient network theories, such as the generalized Green-Tobolsky theory of Tanaka and Edwards [34], rheological parameters such as the zero-shear viscosity and plateau modulus are related directly to the number of elastically active chains per unit volume. In these theories a linear relation is expected between the overall polymer concentration and the plateau modulus. Experimental results however, predict a much stronger increase. According to Annable *et al.* this must be attributed to the fact that not only the number of micelles increases with concentration, but that also the fraction of chains per micelle that forms a bridge (*i.e.* α) is a strong function of concentration [35]. This is exactly what we see in Figure 8.

In this section we have attempted to estimate the polymer concentration where we can expect the first appearance of a macroscopic association cluster of micelles. Of course the criteria used above are static criteria, and do not capture any of the dynamics and possible non-ergodicity of this transition in "real" experimental systems. Application of the results described in this paper, to analyse this transition and its dynamical aspects in more detail, could be an outlook for future research.

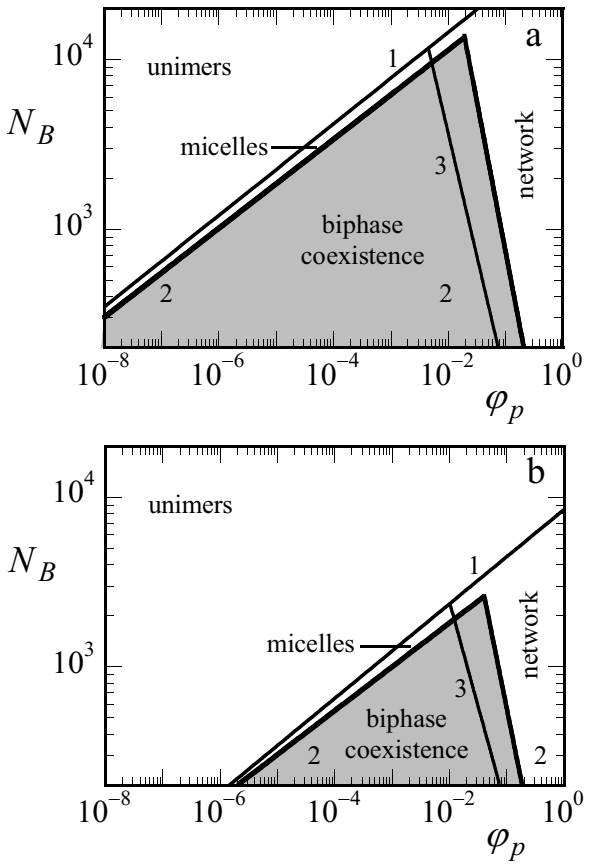

Fig. 10. Phase diagram for A_{20}-B_N-A_{20} (a) and for A_{16}-B_N-A_{16} polymers (b). Indicated transitions are; 1) micellization threshold, 2) the binodal for biphase coexistence and 3) the transient network threshold. Note that the intersect of the two binodal branches is not the actual critical point; it is an upper limit for the critical point.

6 Discussion

With the predictions for the critical micelle concentrations [18], the coexistence curves, and the transient network thresholds, we can construct phase diagrams for our telechelic associative polymers. In Figure 10 we show two examples of phase diagrams, for two values of the end-block length N_A.

In comparing the phase diagrams for $N_A = 20$ and $N_A = 16$, the depression of the upper limit of the critical value of N_B (Eq. (17)) and the shift in the micellization threshold are clearly distinguishable. The volume fractions, corresponding to either the CMC (line 1) or the dilute branch of the binodal (line 2), decrease exponentially with a change in the end-block length N_A (Eqs. (16) and (17)), explaining the large effect for a relatively small change in N_A. For the network formation threshold (line 3), that is proportional to a power-law of N_A, the change is hardly visible.

From Figure 10 and the discussion of the various scaling arguments above, it is clear that there are large differences in how volume fractions, at which the various transitions occur, depend on the molecular architecture. As a result it is not possible to superimpose these phase diagrams by rescaling the volume fraction axis with respect to the volume fraction at the critical point, which is a technique commonly employed when studying phase diagrams.

There is a regime, above the intersection of the micellization threshold with the transient network threshold, where any micelle formation of the associative polymers immediately leads to the formation of a network. This is the case when the middle B block is very long and as a result n_{agg} will typically be very low and the CMC relatively high. As the corona chains can span large distances, any self-assembly will then be accompanied by formation of bridges, leading to a dilute network with nodes, *i.e.* micelles, of low functionality.

As discussed above, we cannot obtain the true critical point in our approach, due to the approximations that were needed to determine coexistence. Of course the binodal should be continuous at the critical point; the true binodal will have a different shape around the critical

point compared to what is shown in Figure 10. We can roughly estimate where our approach is no longer valid. Phase separation no longer occurs when the depth of the attractive minimum in $\Delta F^m(h)$ becomes smaller than the thermal energy k_BT. In other words, conditions where the depth of the attraction is of order k_BT must be close to the critical point. Due to technical issues, it is difficult, in this SF-SCF model, to calculate points close to the critical point. For all points that we have calculated, as shown in Figure 7, we find that the attraction is at least several k_BT. This indicates that for all these results our approach is valid. The regime where we expect the model to break down is very close to the predicted critical point and is too small to indicate in the constructed phase diagrams.

In-depth comparison of our results with existing experimental data, such as in [12,16], is difficult as the experimentally studied range and number of block lengths is too limited to verify the scaling behavior that we predict here. This calls for a systematic experimental investigation of the properties discussed in this paper, over a larger range of both end- and middle block lengths. On a more qualitative level, we find that the experimental studies [12, 16] show the tendency for phase separation to increase when the hydrophobic blocks become longer and/or the hydrophilic blocks smaller. This agrees with our model, *e.g.* see equation (17) and Figure 10.

7 Conclusions

Using a self-consistent field cell model, and explicitly accounting for the self-assembled character of the interacting objects, we have mapped out the self-assembly and phase behavior of telechelic associative polymers with their soluble blocks at θ-conditions. Based on the calculations of intermicellar interactions, coexistence curves were predicted. From the numerical results, the concentration where a transient network is formed, was also predicted. Together with the results for the micellization threshold, phase diagrams were constructed.

Nearly all trends found from the numerical results could be rationalized using relatively simple scaling arguments. With these scaling arguments, a quantitative understanding of how the phase behavior depends on the molecular architecture of the telechelic associative polymers is easily accessible.

The work of J. Sprakel forms part of the research programme of the Dutch Polymer Institute (DPI), project #564.

References

1. J.P. Kaczmarski, J.E. Glass, Macromolecules **26**, 5149 (1993).
2. B. Grassl, L. Billon, O. Borisov, J. Francois, Polym. Int. **55**, 1169 (2006).
3. A.S. Kimerling, W.E. Rochefort, S.R. Bhatia, Ind. Eng. Chem. Res. **45**, 6885 (2006).
4. N. Cathebras, A. Collet, M. Viguier, J.F. Berret, Macromolecules **31**, 1305 (1998).
5. J. Duhamel, A. Yekta, Y.Z. Hu, M.A. Winnik, Macromolecules **25**, 7024 (1992).
6. O. Ortona, G. D'Errico, L. Paduano, V. Vitagliano, J. Colloid Interface Sci. **63**, 301 (2006).
7. X.D. Huang, S.H. Goh, S.Y. Lee, Macromol. Chem. Phys. **201**, 2660 (2000).
8. S.T. Milner, T.A. Witten, Macromolecules **25**, 5495 (1992).
9. D. Cao, J. Wu, Langmuir **22**, 2712 (2006).
10. A. Courvoisier, F. Isel, J. Francois, M. Maaloum, Langmuir **14**, 3727 (1998).
11. S.H. Kim, W. Lau, E. Kumacheva, Macromolecules **33**, 4561 (2000).
12. Q.T. Pham, W.B. Russel, J.C. Thibeault, W. Lau, Macromolecules **32**, 1999 (1999).
13. X.X. Meng, W.B. Russel, J. Rheol. **50**, 169 (2006).
14. S.R. Bhatia, W.B. Russel, Macromolecules **33**, 5713 (2000).
15. A.N. Semenov, J.-F. Joanny, A.R. Kokhlov, Macromolecules **28**, 1066 (1995).
16. J. Francois, E. Beaudoin, O. Borisov, Langmuir **19**, 10011 (2003).
17. A.N. Semenov, M. Rubinstein, Macromolecules **31**, 1373 (1998).
18. J. Sprakel, N.A.M. Besseling, F.A.M. Leermakers, M.A. Cohen Stuart, J. Phys. Chem. B **111**, 2903 (2007).
19. J.M.H.M. Scheutjens, G.J. Fleer, J. Phys. Chem. **83**, 1619 (1979).
20. J.M.H.M. Scheutjens, G.J. Fleer, J. Phys. Chem. **84**, 178 (1980).
21. F.A.M. Leermakers, J. Sprakel, N.A.M. Besseling, P.A. Barneveld, Phys. Chem. Chem. Phys. **9**, 167 (2007).
22. P.J. Flory, *Principles of Polymer Chemistry* (Cornell University Press, Ithaca, 1953).
23. O.A. Evers, J.M.H.M. Scheutjens, G.J. Fleer, Macromolecules **23**, 5221 (1990).
24. F.A.M. Leermakers, J. Lyklema, Colloids Surf. **67**, 239 (1992).
25. B.Y. Zaslavsky, T.O. Bagirov, A.A. Borovskaya, N.D. Gulaeva, L.H. Miheeva, A.U. Mahmudov, M.N. Rodnikova, Polymer **30**, 2104 (1989).
26. T.L. Hill, *Thermodynamics of Small Systems, Parts 1 and 2* (Dover Pub. Inc., New York, 1994).
27. D.G. Hall, B.A. Pethica, in *Nonionic Surfactants*, edited by M.J. Schick (Marcel Dekker Inc., New York, 1967).
28. D.F. Evans, H. Wennerström, *The Colloidal Domain* (Wiley-VCH, New York, 1999).
29. J. Francois, S. Maitre, M. Rawiso, D. Sarazin, G. Beinert, F. Isel, Colloids Surf. A **112**, 251 (1996).
30. M. Daoud, J.P. Cotton, J. Phys. (Paris) **43**, 531 (1982).
31. G. ten Brinke, G. Hadziioannou, Macromolecules **20**, 486 (1987).
32. C. Tanford, *The Hydrophobic Effect; Formation of Micelles and Biological Membranes* (Wiley, New York, 1980).
33. D. Stauffer, J.G. Zabolitzky, J. Phys. A: Math. Gen. **19**, 3705 (1986).
34. F. Tanaka, S.F. Edwards, Macromolecules **25**, 1516 (1992).
35. T. Annable, R. Buscall, R. Ettelaie, D. Whittlestone, J. Rheol. **37**, 695 (1993).